Received: 26 December 2018 | Revised: 29 May 2019 | Accepted: 7 June 2019

DOI: 10.1002/aoc.5089

FULL PAPER

WILEY Applied Organometallic Chemistry

Synthesis, spectra, crystal structures and anticancer studies of 26-membered macrocyclic dibutyltin(IV) dithiocarbamate complexes: Single-source precursors for tin sulfide nanoparticles

Pandurangan Selvaganapathi[1] | Subbiah Thirumaran[1] | Samuele Ciattini[2]

[1] Department of Chemistry, Annamalai University, Annamalinagar 608 002,Tamil Nadu, India

[2] Centro di Cristallografia Strutturale, Polo Scientifio di Sesto Fiorentino, Via della Lastruccia 3, 50019 Sesto Fiorentino, Florence, Italy

Correspondence
S. Thirumaran, Department of Chemistry, Annamalai University, Annamalainagar 608 002, Tamil Nadu, India.
Email: sthirumaran@yahoo.com

Four new macrocyclic dinuclear dibutyltin(IV) dithiocarbamate complexes of the type $[Bu_2Sn(dtc)]_2$, where dtc = hexane-1,6-diylbis(4-fluorobenzyldithiocarbamate) anion (**1**), hexane-1,6-diylbis(4-chlorobenzyldithiocarbamate) anion (**2**), hexane-1,6-diylbis (furfuryldithiocarbamate) anion (**3**) and hexane-1,6-diylbis(pyrrole-2-ylmethyldithiocarbamate) anion (**4**), have been prepared. The dithiocarbamate ligands efficiently self-assemble with $Bu_2Sn(IV)$ to form bimetallic 26-membered macrocycles. All the complexes have been characterized using elemental analysis, infrared and NMR (^1H and ^{13}C) spectroscopies and X-ray crystallography. Single-crystal X-ray diffraction analysis of all the complexes confirms the formation of the dinuclear metallomacrocycles in which dithiocarbamate ligands are asymmetrically bound to the tin atoms. The coordination sphere around the tin atom in **1**–**4** can be described as a skew trapezoidal bipyramid. The dimensions of the cavity of the macrocycles of **1**–**4** are *ca* 8.0×9.0 Å^2. Complexes **1**–**4** were evaluated for their *in vitro* anticancer activity against MCF-7 and HL-60 cells. Complexes **1** and **2** are more active against MCF-7 and HL-60. Thermal decomposition of **1** and **4** yielded tin sulfides. They were characterized using powder X-ray diffraction (PXRD), high-resolution transmission electron microscopy and UV diffuse reflectance and energy-dispersive X-ray spectroscopies. PXRD studies reveal that the as-prepared tin sulfides are composed of orthorhombic phase of SnS.

KEYWORDS
anticancer studies, single-source precursors, tin(IV) dithiocarbamates, tin sulfide nanoparticles

1 | INTRODUCTION

In recent years coordination compounds containing sulfur donor ligands have received considerable attention.[1,2] Among these ligands, dithiocarbamates have attracted attention owing to their importance in the preparation of a variety of metal complexes in various oxidation states and coordination geometries.[3–5] Complexes of dithiocarbamate ligands have various applications in vulcanization accelerators, analysis, radiation protectors and as precursors for the preparation of metal sulfide and metal oxide nanoparticles.[6–10] Interest in organotin dithiocarbamate complexes arises because of their variety of structures and wide range of applications in fields such as agriculture,

biology, organic synthesis and catalysis.[11–13] The products obtained from the reaction of organtin(IV) halides with dithiocarbamates show substantial tendency to generate self-assembled supramolecular architectures[14,15] and can also offer a platform for the formation of macrocyles[16–18] due to the Lewis acidity of organotin(IV) chlorides. In terms of crystallographic analyses, the diorganotin(IV) dithiocarbamates are the best studied and arguably the most interesting in terms of the observed structural diversity. These complexes show that there are four distinct structural motifs.[19–23] Recent studies have shown very promising *in vitro* antitumour properties of organotin compounds against a wide panel of tumour cell lines of human origin. In some cases, diorganotin(IV) derivatives have also shown acceptable *in vivo* antiproliferative activity as new chemotherapy agents.[13,24,25] In addition, these complexes have been found to be efficient and somewhat selective anion and cation receptors.[26–30] Recently, investigations in the field of photovoltaics have been directed towards the development of cost-effective and non-toxic materials for solar cell fabrication. Tin sulfide is one such compound that belongs to the group IV–VI semiconductors. It has attracted particular attention as a low-toxicity solar energy absorber,[31,32] in halographic recording[33,34] and for infrared detection.[35] Organotin(IV) dithiocarbamates are widely used as single-source precursors for the preparation of tin sulfide nanomaterials (SnS, SnS_2 and SnS_3).[36–38] The organic substituents on the dithiocarbamate ligands play an important role in determining the biological activities of the organotin dithiocarbamate complexes[11,13] and the phase, size and shape of metal sulfides prepared from such metal dithiocarbamate complexes.[10,36–38]

In consideration of all the above facts, our aim was to prepare macrocyclic diorganotin(IV) dithiocarbamate complexes containing various N-bound organic moieties (fluorobenzyl, chlorobenzyl, furfuryl and pyrrole) to study the effect of such organic moieties on anticancer activity of the complexes and properties of tin sulfide nanoparticles prepared from the complexes. In this paper, the preparation, spectral and structural characterization and anticancer activity of four 26-membered macrocyclic diorganotin(IV) bis(dithiocarbamate) complexes are reported. In addition, tin sulfide nanoparticles were prepared from two of the complexes.

2 | EXPERIMENTAL

2.1 | Materials and methods

All reagents and solvents were used as received without further purification and all experiments were carried out in atmospheric air. Melting points were determined using an electro-thermal melting point apparatus and are uncorrected. Microanalysis for carbon, hydrogen and nitrogen in the synthesized complexes was conducted with a Vario MICRO V2.2.0 elemental analyser. Fourier transform infrared (FT-IR) spectra were recorded with a PerkinElmer FT-IR spectrometer. NMR spectra were recorded with Bruker 400 MHz (^{1}H and ^{13}C) and Bruker 500 MHz (^{119}Sn) spectrometers at room temperature in $CDCl_3$ as a solvent, using tetramethylsilane as an internal standard. Thermogravimetric analysis (TGA) was performed using a NETZSCH 5 thermal instrument. Samples were heated at a rate of 10°C min^{-1}. Powder X-ray diffraction (XRD) patterns were recorded using an EQUINX 1000. High-resolution transmission electron microscopy (HRTEM) images were recorded using a Jeol JEM2100 (200 keV and LaB6 filament) and energy-dispersive X-ray spectroscopy (EDS) was conducted using INCA energy software. Diffuse reflectance spectra were recorded using a JASCO V-670 UV–visible spectrophotometer.

2.2 | X-ray crystallography

Single-crystal X-ray diffraction data for complexes **1** and **2** were obtained with an Xcalibur Onyx (Cu Kα radiation (λ = 1.54184 Å)) diffractometer and those for complexes **3** and **4** with an Xcalibur Sapphire 3 (Mo Kα radiation (λ = 0.71073 Å)) diffractometer. The structures were solved and refined by direct method using SHELXL-2014/7.[39] Details of the data collection, crystal data and structure refinement parameters for **1**–**4** are given in Table 1.

2.3 | Anticancer activity (procedure for sulforhodamine B (SRB) assay)

Cell lines were grown in RPMI 1640 medium containing 10% foetal bovine serum and 2 mM L-glutamine. For screening experiments, cells were inoculated into 96-well microtiter plates in 100 μl at plating densities as shown in the study details above, depending on the doubling time of individual cell lines. After cell inoculation, the microtiter plates were incubated at 37°C, 5% CO_2, 95% air and 100% relative humidity for 24 h prior to addition of experimental drugs.

Experimental drugs were initially solubilized in dimethylsulfoxide at 100 mg ml^{-1} and diluted to 1 mg ml^{-1} using water and stored frozen prior to use. At the time of drug addition, an aliquot of frozen concentrate (1 mg ml^{-1}) was thawed and diluted to 100, 200, 400 and 800 μg ml^{-1} with complete medium containing test

TABLE 1 Crystal data, data collection and refinement parameters for **1–4**

	1	2	3	4
Empirical formula	$C_{62}H_{84}F_4N_5S_8Sn_2$	$C_{60}H_{84}Cl_4N_4S_8Sn_2$	$C_{52}H_{80}N_4O_4S_8Sn_2$	$C_{54}H_{86}C_{26}N_8S_8Sn_2$
Formula weight	1469.2	1496.96	1319.06	1553.86
Crystal dimensions (mm^3)	0.15 × 0.10 × 0.05	0.35 × 0.30 × 0.28	0.25 × 0.23 × 0.20	0.27 × 0.25 × 0.20
Crystal system	Monoclinic	Monoclinic	Monoclinic	Triclinic
Space group	C2/c	$P2_1/c$	$P2_1/n$	Pī
a (Å)	44.344(3)	18.0714(6)	15.3807(16)	10.3288(4)
b (Å)	10.5351(5)	11.7027(5)	9.6617(3)	10.9333(4)
c (Å)	16.8311(7)	16.3041(5)	20.7559(19)	16.6210(6)
α (°)	90	90	90.000	102.679(3)
β (°)	118.220(3)	95.432(3)	92.221(7)	106.164(3)
γ (°)	90	90	90.000	97.945(3)
V ($Å^3$)	6928.4(7)	3432.6(2)	3082.1(4)	1718.56(12)
Z	4	4	4	2
D_c (g cm^{-3}	1.409	1.448	1.421	1.501
μ (cm^{-1})	—	9.792	1.125	1.244
$F(000)$	3020	1536	1360	796
λ (Å)	Cu K_α (1.54184)	Cu K_α (1.54184)	Mo K_α (0.71073)	Mo K_α (0.71069)
θ range (°)	4.35–72.32	4.50–72.16	4.332–29.048	4.116–31.026
Index ranges	$-53 \le h \le 53$, $-12 \le k \le 9$, $-20 \le l \le 18$	$-22 \le h \le 16$, $-14 \le k \le 14$, $-19 \le l \le 19$	$-19 \le h \le 20$, $-13 \le k \le 11$, $-28 \le l \le 27$	$-13 \le h \le 14$, $-15 \le k \le 15$, $-22 \le l \le 22$
Reflections collected	14 973	15 496	10 919	27 235
Observed reflections [$I > 2\sigma(I)$]	4388	5181	5724	7907
Weighting scheme	Calcd $w = 1/[\sigma^2(F_o^2) + (0.0847P)^2]$, where $P = (F_o^2 + 2F_c^2)/3$	Calcd $w = 1/[\sigma^2(F_o^2) + (0.1021P)^2 + 9.1503P]$, where $P = (F_o^2 + 2F_c^2)/3$	Calcd $W = 1/(\sigma^2(F_o^2) + (0.0254p)^2 + 12.8424p)$, where $p = (F_o^2 + 2F_c^2)/3$	Calcd $W = 1/(\sigma^2(F_o^2) + (0.0341p)^2 + 0.1947p)$, where $p = (F_o^2 + 2F_c^2)/3$

(Continues)

TABLE 1 (Continued)

	1	2	3	4
Number of parameters refined	358	352	310	524
$R[F^2 > 2\sigma(F^2)]$, $wR(F^2)$	0.0536, 0.1732	0.0625, 0.1953	0.0544, 0.1229	0.0389, 0.0815
GOOF	1.00	1.019	1.042	0.998

sample. Aliquots of 10 μl of these different drug dilutions were added to the appropriate microtiter wells already containing 90 μl of medium, resulting in the required final drug concentrations, i.e.10, 20, 40 and 80 μg ml^{-1}. After compound addition, plates were incubated at standard conditions for 48 h and assay was terminated by the addition of cold TCA. Cells were fixed *in situ* by the gentle addition of 50 μl of cold 30% (w/v) TCA (final concentration, 10% TCA) and incubated for 60 min at 4°C. The supernatant was discarded; the plates were washed five times with tap water and air dried. SRB solution (50 μl) at 0.4% (w/v) in 1% acetic acid was added to each of the wells, and plates were incubated for 20 min at room temperature. After staining, unbound dye was recovered and the residual dye was removed by washing five times with 1% acetic acid. The plates were air-dried. Bound stain was subsequently eluted with 10 mM trizma base, and the absorbance was read on a plate reader at a wavelength of 540 nm with 690 nm reference wavelength.

Percent growth was calculated on a plate-by-plate basis for test wells relative to control wells. Percent growth was expressed as the ratio of average absorbance of the test well to the average absorbance of the control wells × 100. Using the six absorbance measurements (time zero (Tz), control growth (C) and test growth in the presence of drug at the four concentration levels (Ti)), the percentage growth was calculated at each of the drug concentration levels. Percentage growth inhibition was calculated as: [Ti/C] × 100%.

2.4 | Preparation of macrocyclic dibutyltin(IV) dithiocarbamate complexes

2.4.1 | Preparation of *N*,*N*′-disubstituted hexamethylene-1,6-diamines

1,6-Hexamethylenediamine (4.6 mmol) and two equivalents of aldehyde (4-fluorobenzaldehyde, 4-chlorobenzaldehyde, furfuraldehyde and pyrrole-2-carboxaldehyde) (10.6 mmol) were dissolved in ethanol (30 ml) and the reaction mixture was refluxed for 2 h. After evaporation of the solvent the diimine was obtained in the form of a yellow liquid. The *N*,*N*′-disubstituted hexamethylene-1,6-diimine was dissolved in methanol and kept in an ice bath to which a solution of $NaBH_4$ (27.6 mmol) in methanol (30 ml) was added dropwise with stirring. Stirring was continued for 12 h. After the removal of the solvent by evaporation, the resulting viscous liquid was washed with water. The product was extracted using dichloromethane. Evaporation of dichloromethane afforded *N*,*N*′-disubstituted hexamethylene-1,6-diamine as yellow oil.[18]

2.4.2 | Preparation of bis(μ_2-hexane-1,6-diylbis((4-fluorobenzyl) dithiocarbamato)-κ^4S,S',S'',S''')tetra-*n*-butylditin(IV) (1)

N,*N*′-Di(4-fluorobenzyl)hexamethylene-1,6-diamine (4.0 mmol) and two equivalents of triethylamine (8.0 mmol) were dissolved in ethanol (30 ml) whereupon an excess of carbon disulfide (12.0 mmol) was added. After the mixture was stirred for 2 h at room temperature, a solution of one equivalent of dibutyltin dichloride (4.0 mmol) in methanol (20 ml) was added giving almost immediately a white precipitate. The precipitate was separated by filtration and washed with water (Scheme 1). Yield: 75%; m.p. 146–148°C. Anal. Calcd for $C_{60}H_{84}F_4N_4S_8Sn_2$ (%): C, 50.35; H, 5.92; N, 3.91. Found (%): C, 50.14; H, 5.93; N, 3.87. FT-IR (cm^{-1}) with KBr disc: 1478 (νC–N), 981 (νC–S). ^{1}H NMR (400 MHz, $CDCl_3$, δ, ppm): 0.95 (t, 12H, J = 7.6 Hz, $CH_3CH_2CH_2CH_2Sn$); 1.22 (b, 8H, $CH_2CH_2CH_2N$); 1.39–1.51 (m, 8H, $CH_2CH_2CH_2Sn$); 1.68 (b, 8H, CH_2CH_2N); 1.91–1.99 (m, 8H, CH_2CH_2Sn); 2.12 (t, 8H, J = 8.8 Hz, CH_2Sn); 3.63 (t, 8H, J = 8.4 Hz, CH_2N); 5.14 (s, 8H, $4FC_6H_4CH_2N$); 7.00–7.28 (phenyl ring protons). ^{13}C NMR: 13.9 ($CH_3CH_2CH_2CH_2Sn$); 26.4 ($CH_2CH_2CH_2Sn$); 26.8 ($CH_2CH_2CH_2N$); 28.6 (CH_2CH_2N); 29.7 (CH_2CH_2Sn); 34.0 (CH_2Sn); 53.9 (CH_2N); 56.6 ($4FC_6H_4CH_2N$); 115.5, 115.7, 129.3, 131.5 (phenyl ring carbons); 161.2, 163.6 (4F—Ar); 202.1 (NCS_2).

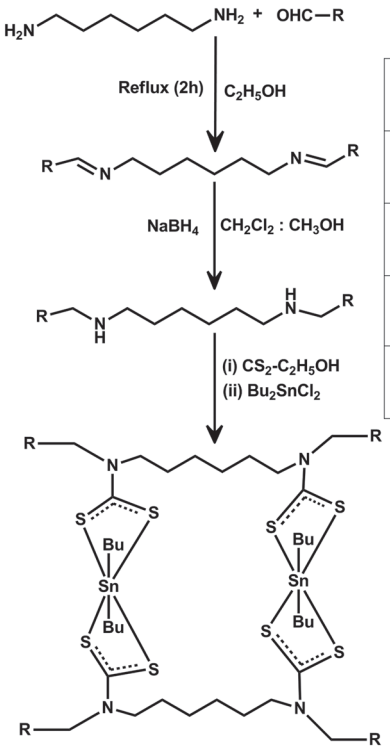

Complex	R
1	F
2	Cl
3	O
4	N H

SCHEME 1 Preparation of dibutyltin(IV) dithiocarbamate complexes **1**–**4**

2.4.3 | Preparation of bis(μ_2-hexane-1,6-diylbis((4-chlorobenzyl) dithiocarbamato)-κ^4S,S',S'',S''')tetra-*n*-butylditin(IV) (2)

A method similar to that described for the synthesis of **1** was adopted; however, *N*,*N*-di(4-chlorobenzyl) hexamethylene-1,6-diamine was used instead of *N*,*N*-di(4-fluorobenzyl)hexamethylene-1,6-diamine. Yield: 76%; m.p. 142–144°C. Anal. Calcd for $C_{60}H_{84}Cl_4N_4S_8Sn_2$ (%): C, 48.14; H, 5.66; N, 3.74. Found (%): C, 47.99; H, 5.63; N, 3.72. FT-IR (cm^{-1}) with KBr disc: 1477 (νC–N), 980 (νC–S). ^{1}H NMR (400 MHz, $CDCl_3$, δ, ppm): 0.95 (t, 12H, J = 7.2 Hz, $CH_3CH_2CH_2CH_2Sn$); 1.23 (b, 8H, $CH_2CH_2CH_2N$); 1.44–1.51 (m, 8H, $CH_2CH_2CH_2Sn$); 1.69 (b, 8H, CH_2CH_2N); 1.88–1.95 (m, 8H, CH_2CH_2Sn); 2.11 (t, 8H, J = 5.6 Hz, CH_2Sn); 3.63 (t, 8H, J = 8.0 Hz, CH_2N); 5.13 (s, 8H, $4ClC_6H_4CH_2N$); 7.20–7.36 (phenyl ring protons). ^{13}C NMR: 14.0 ($CH_3CH_2CH_2CH_2Sn$); 26.4 ($CH_2CH_2CH_2Sn$); 26.8 ($CH_2CH_2CH_2N$); 28.6 (CH_2CH_2N); 29.7 (CH_2CH_2Sn); 33.9 (CH_2Sn); 54.1 (CH_2N); 56.7 ($4ClC_6H_4CH_2N$); 127.6, 127.8, 128.8, 128.9, 133.6, 134.1, 134.3, 135.7 (phenyl ring carbons), 202.3 (NCS_2).

2.4.4 | Preparation of bis(μ_2-hexane-1,6-diylbis((furfuryl)dithiocarbamato)-κ^4S,S',S'',S''')tetra-*n*-butylditin(IV) (3)

A method similar to that described for the synthesis of **1** was adopted; however, *N*,*N*-di (furfuryl)hexamethylene-1,6-diamine was used instead of *N*,*N*-di(4-fluorobenzyl) hexamethylene-1,6-diamine. Yield: 79%; m.p. 128–130°C. Anal. Calcd for $C_{52}H_{80}N_4O_4S_8Sn_2$ (%): C, 47.35; H, 6.11; N, 4.25. Found (%): C, 47.21; H, 6.07; N, 4.26. FT-IR (cm^{-1}) with KBr disc: 1473 (νC–N), 980 (νC–S). ^{1}H NMR (400 MHz, $CDCl_3$, δ, ppm): 0.92 (t, 12H, J = 7.2 Hz, $CH_3CH_2CH_2CH_2Sn$); 1.25 (b, 8H, $CH_2CH_2CH_2N$); 1.41–1.46 (m, 8H, $CH_2CH_2CH_2Sn$); 1.66 (b, 8H, CH_2CH_2N); 1.89–1.95 (m, 8H, CH_2CH_2Sn); 2.07 (t, 8H, J = 8.0 Hz, CH_2Sn); 3.72 (t, 8H, J = 8.0 Hz, CH_2N); 5.07 (s, 8H, (furfuryl)CH_2N); 6.34–7.37 (furyl ring protons). ^{13}C NMR: 13.9 ($CH_3CH_2CH_2CH_2Sn$); 26.5 ($CH_2CH_2CH_2Sn$); 26.9 ($CH_2CH_2CH_2N$); 28.6 (CH_2CH_2N); 29.7 (CH_2CH_2Sn); 33.8 (CH_2Sn); 54.4 (CH_2N); 50.3 ((furfuryl)CH_2N); 109.6, 110.7, 142.3, 149.3 (furyl ring carbons); 201.6 (NCS_2).

2.4.5 | Preparation of bis(μ_2-hexane-1,6-diylbis((pyrrole-2-ylmethyl) dithiocarbamato)-κ^4S,S',S'',S''')tetra-*n*-butylditin(IV) (4)

A method similar to that described for the synthesis of **1** was adopted; however, *N*,*N*-di(pyrrole-2-ylmethyl) hexamethylene-1,6-diamine was used instead of *N*,*N*-di(4-fluorobenzyl)hexamethylene-1,6-diamine. Yield: 73%; m.p. 148–150°C. Anal. Calcd for $C_{52}H_{84}N_8S_8Sn_2$ (%): C, 47.49; H, 6.44; N, 8.52. Found (%): C, 47.38; H, 6.44; N, 8.50. FT-IR (cm^{-1}) with KBr disc: 1482 (νC–N), 977 (νC–S). ^{1}H NMR (400 MHz, $CDCl_3$, δ, ppm): 0.95 (t, 12H, J = 7.6 Hz, $CH_3CH_2CH_2CH_2Sn$); 1.27 (b, 8H, $CH_2CH_2CH_2N$); 1.44–1.49 (m, 8H, $CH_2CH_2CH_2Sn$); 1.70 (b, 8H, CH_2CH_2N); 1.89–1.96 (m, 8H, CH_2CH_2Sn); 2.11 (t, 8H, J = 9.2 Hz, CH_2Sn); 3.65 (t, 8H, J = 8.4 Hz, CH_2N); 4.98 (s, 8H, (pyrrole)CH_2N); 6.10–6.76 (pyrrole ring protons); 9.40 (s, 4H, pyrrole NH). ^{13}C NMR: 13.9 ($CH_3CH_2CH_2CH_2Sn$); 26.4 ($CH_2CH_2CH_2Sn$); 26.9 ($CH_2CH_2CH_2N$); 27.0 (CH_2CH_2N); 28.6 (CH_2CH_2Sn); 33.5 (CH_2Sn); 54.2 (CH_2N); 50.9 ((pyrrole)CH_2N); 107.5, 108.8, 118.7, 126.9 (pyrrole ring carbons); 200.7 (NCS_2).

2.5 | Preparation of tin sulfide nanoparticles

Tin sulfide nanoparticles obtained from complexes **1** and **4** are represented by SnS-1 and SnS-2.

2.5.1 | Preparation of SnS-1

An amount of 1.5 g of complex **1** was placed in a muffle furnace at 330°C for 30 min in the presence of air atmosphere. The final residue was analysed to SnS-1.

2.5.2 | Preparation of SnS-2

An amount of 1.5 g of complex **4** was placed in a muffle furnace at 250°C for 30 min in the presence of air atmosphere. The final residue was analysed to SnS-2.

3 | RESULTS AND DISCUSSION

3.1 | Spectral studies and TGA

FT-IR and NMR (H^1, ^{13}C and ^{119}Sn) spectra of complexes **1–4** are shown in Figures S1–S14. The FT-IR spectra of complexes **1–4** exhibit bands characteristic for tin-coordinated dithiocarbamate group. The vibrations for the N—C (thioureide) bonds of the dithiocarbamate ligands in **1–4** gave bands at positions intermediate between those of a single and a double bond (1473–1482 cm^{-1}), which can be attributed to the delocalization of π-electron density within the NCS_2 group of atoms.[40] In the spectra of the investigated complexes, the vibrational modes of CS_2 are of particular interest to differentiate between monodentate and bidentate coordination of the dithiocarbamate moiety. A single band which appeared around 980 cm^{-1} for complexes **1–4** corresponds to ν_{C-S} vibration and indicates bidentate coordination mode of the dithiocarbamate moiety through the two S donor atoms.[41]

The ^{1}H NMR spectra for the $Bu_4Sn_2L_2$ (L = dithiocarbamate ligand) macrocycle show both L^{2-} units to be magnetically equivalent; moreover, the two halves in each L^{2-} are also equivalent, showing one set of signals for one-fourth of the complex. The ^{1}H NMR spectra of all four complexes exhibit a triplet and a singlet in the ranges 3.63–3.72 and 4.98–5.14 ppm for NCH_2 of hexamethylene group and another NCH_2 group attached to the aromatic ring, respectively. Two broad signals observed around 1.25 and 1.68 ppm are assigned to $CH_2CH_2CH_2N$ and $CH_2CH_2CH_2N$, respectively. The methylene group attached to tin atom shows a triplet at around 2.10 ppm. Another triplet observed at around 0.95 ppm and two multiplets in the ranges 1.39–1.51 and 1.89–1.99 ppm are due to methyl protons and the remaining two methylene protons of butyl group, respectively. Aromatic protons exhibit signals in the region 6.10–7.37 ppm. In the case of **4**, NH proton of pyrrole group appeared at 9.40 ppm.

In the ^{13}C NMR spectra, the assignment of the ^{13}C signal for CS_2 group in all the complexes is quite straightforward and is observed in the range 200.7–202.3 ppm indicating the coordination of sulfur atoms with the tin atom.[42,43] The methylene carbon attached to the tin atom gave signals in the range 33.5–34.0 ppm. The complexes exhibit ^{13}C NMR signals for NCH_2 carbon attached to aromatic ring at 56.6, 56.7, 50.3 and 50.9 ppm for **1–4**, respectively, while the NCH_2 carbons bound to the hexamethylene chain are found to resonate at around 54.0 ppm. Signals of the butyl carbon atoms appeared at around 13.9, 26.4, 29.0 and 34.0 ppm. The signals observed in the region 107.5–163.6 ppm are assigned to the aromatic carbons.

In order to study the coordination environment around tin in solution, ^{119}Sn NMR spectra for complexes **1** and **2** were recorded in $CDCl_3$ solution at room temperature. For **1** and **2**, ^{119}Sn chemical shifts appeared at −332.3 and −331.9 ppm, respectively. As reported previously, four-, five- and six-coordinated tin compounds have ^{119}Sn chemical shifts in the ranges +200 to −60 ppm, −90 to −190 ppm and −210 to −400 ppm,

respectively.[44] Therefore, ^{119}Sn chemical shifts of **1** (−332.3 ppm) and **2** (−331.9 ppm) show that Sn atoms in complexes **1** and **2** are hexa-coordinated.

Thermal decomposition of complex **1** was studied using TGA. The overlapped TG/DTG curves are shown in Figure 1. Two-step decomposition in the ranges 240–325 and 420–560°C was observed. The first decomposition step occurred with weight loss of 65.3%. This weight loss corresponds to the decomposition of the organic moiety in the complexes and the formation of metal thiocyanate intermediate (% of residue: expt. 34.7 and calcd 32.0%). This intermediate decomposed in the range 420–560°C. The final residue is 19.6% which is in good agreement with calculated value of 20.5% for SnS. TGA studies of similar $[Bu_2Sn(dtc)_2]$ were carried out under air and nitrogen atmosphere. In these cases also, the final residue is SnS.[45–47]

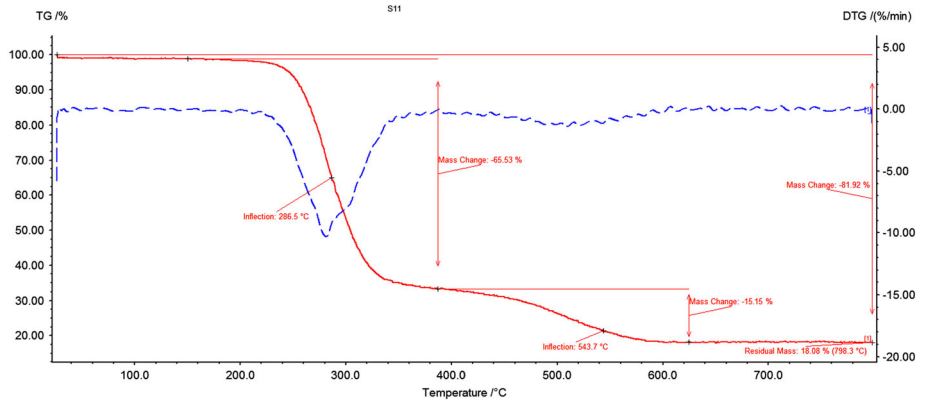

FIGURE 1 TG and DTC curves of **1**

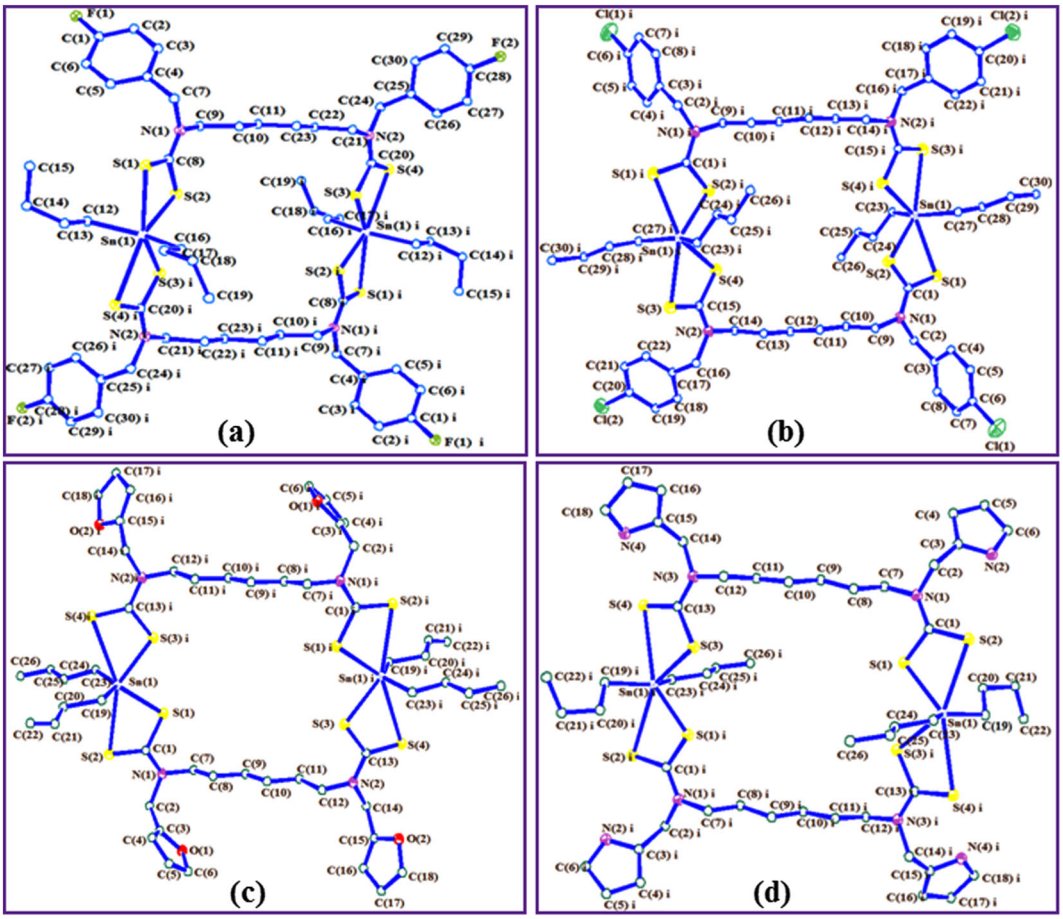

FIGURE 2 ORTEP diagrams of **1–4**

3.2 | Single-crystal X-ray structural analysis of 1–4

ORTEP diagrams of **1–4** with numbering scheme are shown in Figure 2. Selected bond lengths and bond angles are given in Table 2. Complexes **1–4** have dinuclear 26-membered macrocyclic structures and display symmetry, each being disposed about a crystallographic centre of inversion. As can be seen from the structures (Figure 2), the dithiocarbamate ligands bind to the metal primarily in a monodentate fashion. Several organotin complexes containing one or more dithiocarbamates are known which reveal that these ligands are rarely symmetrically bound to the tin.[42,43] In these complexes one sulfur atom of each dithiocarbamate forms a normal covalent bond with Sn (Sn–S = 2.4911(10)–2.5317(16) Å). The distances between the Sn atom and the other sulfur atoms of dithiocarbamate ligands are in the range 2.985(1)–3.138(1) Å, which are longer than the covalently bonded Sn–S distance and significantly less than the sum of van der Waals radii of

TABLE 2 Selected bond distances and bond angles for **1–4**

1		**2**		**3**		**4**	
Bond distance (Å)		**Bond distance (Å)**		**Bond distance (Å)**		**Bond distance (Å)**	
	XRD		**XRD**		**XRD**		**XRD**
Sn1–C12	2.146(7)	Sn1–C27	2.153(7)	Sn1–C19	1.972(13)	Sn1–C19	2.141(3)
Sn1–C16	2.159(7)	Sn1–C23	2.162(7)	Sn1–C23	2.256(8)	Sn1–C23	2.143(3)
Sn1–S2	2.5156(18)	S1–Sn1	2.943(2)	Sn1–S1	2.4911(10)	Sn1–S1	2.5203(6)
Sn1–S3	2.5265(18)	Sn1–S2	2.5181(17)	Sn1–S2	2.936(2)	Sn1–S2	2.9854(7)
Sn1–S1	2.933(2)	Sn1–S3	2.9199(18)	Sn1–S3	2.5041(13)	Sn1–S3	2.5210(6)
Sn1–S4	2.962(2)	Sn1–S4	2.5317(16)	Sn1–S4	3.138(1)	Sn1–S4	3.0473(7)
S1–C8	1.705(7)	S1–C1	1.703(6)	S1–C1	1.739(4)	S1–C1	1.742(2)
S2–C8	1.750(7)	S2–C1	1.738(7)	S2–C1	1.682(4)	S2–C1	1.696(2)
S3–C20	1.760(7)	S3–C15	1.699(6)	S3–C13	1.736(4)	S3–C13	1.735(2)
S4–C20	1.700(7)	S4–C15	1.744(6)	S4–C13	1.693(4)	S4–C13	1.709(2)
N1–C8	1.318(9)	N1–C1	1.349(9)	N1–C1	1.339(5)	N3–C13	1.337(3)
N2–C20	1.322(9)	N2–C15	1.330(8)	N2–C13	1.344(5)	N1–C1	1.339(3)
Bond angle (°)		**Bond angle (°)**		**Bond angle (°)**		**Bond angle (°)**	
C12–Sn1–C16	137.9(3)	C27–Sn1–C23	142.0(3)	C19A–Sn1–C23A	134.2(5)	C19–Sn1–C23	136.91(10)
C12–Sn1–S2	105.9(2)	C27–Sn1–S2	107.1(2)	C19A–Sn1–S1	113.5(4)	C19–Sn1–S1	109.18(7)
C16–Sn1–S2	104.6(2)	C23–Sn1–S2	103.1(2)	C23A–Sn1–S1	104.6(2)	C23–Sn1–S1	103.92(8)
C12–Sn1–S3	109.9(2)	C27–Sn1–S4	102.19(19)	C19A–Sn1S1	100.6(2)	C19–Sn1–S3	106.41(8)
C16–Sn1–S3	102.1(2)	C23–Sn1–S4	103.3(2)	C23A–Sn1–S3	96.4(2)	C23–Sn1–S3	104.35(7)
S2–Sn1–S3	83.06(6)	C27–Sn1–S3	81.7(2)	S2–Sn1–S1	65.21(4)	S1–Sn1–S3	82.85(2)
S1–Sn1–S2	65.66(6)	C23–Sn1–S3	83.6(2)	S3–Sn1–S4	62.53(3)	S3–Sn1–S4	64.12(2)
S3–Sn1–S4	65.21(6)	S2–Sn1–S3	149.97(5)	S1–Sn1–S3	80.89(4)	S2–Sn1–S1	64.65(2)
S1–C8–S2	118.8(4)	S4–Sn1–S3	65.74(5)	S2–C1–S1	119.0(2)	S2–C1–S1	119.53(14)
S4–C20–S3	118.9(4)	S2–Sn1–S1	65.62(5)	S4–C13–S3	120.5(2)	S4–C13–S3	120.47(14)
N1–C8–S1	123.8(5)	S2–Sn1–S4	84.25(5)	N1–C1–S2	123.9(3)	N1–C1–S2	122.29(18)
N1–C8–S2	117.4(5)	S1–C1–S2	120.0(4)	N1–C1–S1	117.1(3)	N1–C1–S1	118.16(17)
N2–C20–S4	123.4(5)	S3–C15–S4	119.7(4)	N2–C13–S4	124.1(3)	N3–C13–S4	121.77(18)
N2–C20–S3	117.7(5)	N1–C1–S1	122.2(5)	N2–C13–S3	115.4(3)	N3–C13–S3	117.76(17)
		N1–C1–S2	117.8(5)				
		N2–C15–S4	117.5(5)				
		N2–C15–S3	122.8(5)				

3.97 Å.[48] The Sn–C bonds (Sn–C = 2.141(3)–2.162(7) Å) are well within the usually observed Sn–C distances in organotin compounds. The coordination sphere around the tin atoms in these complexes can be described as a slightly distorted tetrahedron. However, if the two long Sn–S bonds are taken into account, tin atoms have skewed trapezoidal bipyramidal coordination environments. The four sulfur atoms constitute a trapezoid and the two carbon atoms of butyl occupy the axial positions to complete the six-coordination of the tin atom. The effective cavity size of **1**–**4** is *ca* 8.0 × 9.0 $Å^2$ (Figure 3). The length of the C–S bond is inversely correlated with the Sn–S bond; thus short S–C bonds (C–S = 1.682(4)–1.709(2) Å) and long S–C bonds (C–S = 1.735(2)–1.760(7) Å) correlate with long and short Sn–S bonds, respectively. All C–S bond lengths are significantly shorter than the C–S single bond (*ca* 1.81 Å) due to π-delocalization over the NCS_2 units.[19–23] Within the dithiocarbamate function, the C–N_{dtc} bond lengths in the range 1.318(9)–1.349(9) Å indicate a substantial delocalization of π-electron density in this bond.[14–18]

The crystal structure of **1** is further stabilized through two C–H···F interactions (Figure 4). Intramolecular weak C–H···S interactions are present in this compound which can be seen in Figure S15. Complex **2** is stabilized by C–H···Cl intermolecular interactions with H···Cl = 2.827 Å, which gives rise to a supramolecular network in the solid state (Figure 5). The supramolecular structure is further stabilized by C–H···S interactions (Figure S16). Complex

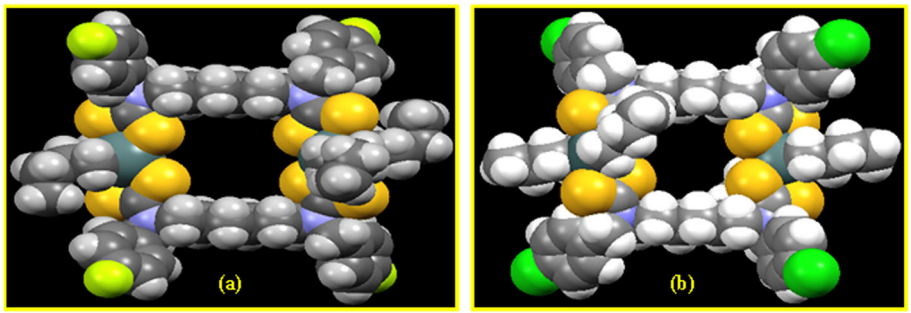

FIGURE 3 Space filling model of (a) **1** and (b) **2** showing the macrocyclic cavity

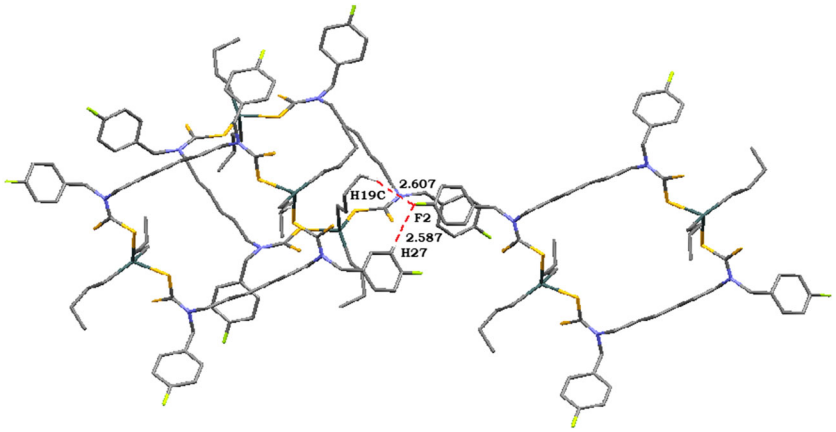

FIGURE 4 Intermolecular C–H···F interactions in **1**

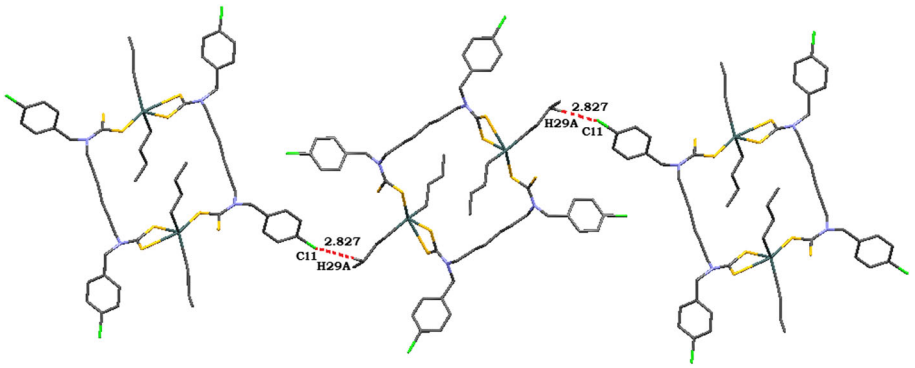

FIGURE 5 Intermolecular C–H···Cl interactions in **2**

TABLE 3 Geometric details of hydrogen bonding (Å, °) in complexes **1–4**

Interaction	D–H	H···A	D···A	D–H···A	Interaction	D–H	H···A	D···A	D–H···A
1							**3**		
C19–H19C···F2[a]	0.96	2.607	3.529	160.77	C7–H7A···S1[a]	0.97	2.565	2.936	102.78
C27–H27···F2[a]	0.93	2.587	3.463	157.07	C2–H2A···S2[a]	0.97	2.526	3.042	113.27
C7–H7A···S1[b]	0.97	2.540	3.060	113.50	C12–H12A···S3[a]	0.97	2.480	2.901	105.88
C9–H9A···S2[b]	0.97	2.498	2.963	109.23	C14–H14B···S4[a]	0.97	2.541	3.075	114.65
C21–H21B···S3[b]	0.97	2.562	2.946	103.70			**4**		
C24–H24B···S4[b]	0.97	2.583	3.081	111.97	C23–H23B···S2[a]	0.84	2.994	3.396	111.82
2					C7–H7A···S1[b]	0.93	2.558	2.971	107.58
C29–H29A···Cl[a]	0.97	2.827	3.644	142.59	C2–H2B···S2[b]	0.95	2.640	3.031	105.33
C9–H9A···S3[a]	0.97	2.859	3.544	128.53	C12–H12A···S3[b]	0.96	2.484	2.953	109.94
C2–H2A···S1[b]	0.97	2.518	3.031	112.93	C14–H14A···S4[b]	1.01	2.598	3.017	104.57
C9–H9A···S2[b]	0.97	2.506	2.938	106.98					
C16–H16A···S3[b]	0.97	2.568	3.038	109.86					
C14–H14A···S4[b]	0.97	2.588	2.969	103.58					

[a]Intermolecular C–H···S interaction.

[b]Intramolecular C–H···S interaction.

2 has four more intramolecular C–H···S interactions (Figure S17). In complex **3**, there are no significant intermolecular interactions. However, intramolecular C–H···S interactions are observed (Figure S18; Table 3). The neighbouring molecules are linked by intermolecular C–H···S interactions between H23B (methylene proton of butyl group) and S2 atom, generating a linear chain. These interactions also form a 12-membered macrocyclic ring (Figure 6). All the S atoms of CS_2 group are involved in the formation of intramolecular C–H···S bonds with H atoms of methylene groups adjacent to N atom of dithiocarbamate ligand (Figure S19; Table 3).

3.3 | Anticancer activity

The *in vitro* anticancer activity of complexes **1–4** was analysed against MCF-7 and HL-60 cells and was evaluated in terms of GI_{50} (concentration of drug that produces 50% inhibition of cells), TGI (concentration of drug that produces total inhibition of cells) and LC_{50} (median lethal concentration) using SRB assay. The growth rate curves are shown in Figure 7. The observed results revealed that complexes **1** and **2** show pronounced GI_{50} values <10 μg ml^{-1} towards both the tested cell lines (Table S1). Complex **3** shows lower activity (GI_{50} > 80 μg ml^{-1}) against both cell lines than the other complexes, while complex **4** reveals moderate activity against MCF-7 and better activity against HL-60.

3.4 | Characterization of tin sulfide nanoparticles

Figure 8 shows the XRD patterns of SnS-1 and SnS-2 prepared by thermal decomposition of complexes **1** and **4**, respectively. The XRD patterns exhibit multiple intense peaks that are clearly distinguishable. The diffraction

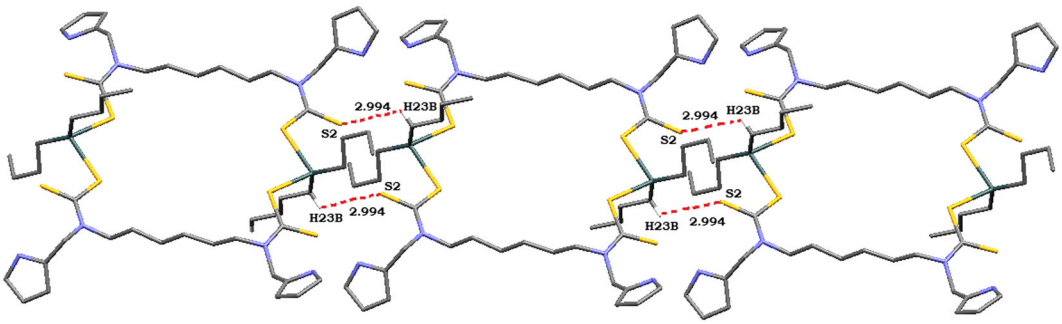

FIGURE 6 Intermolecular C–H···S interactions in **4**

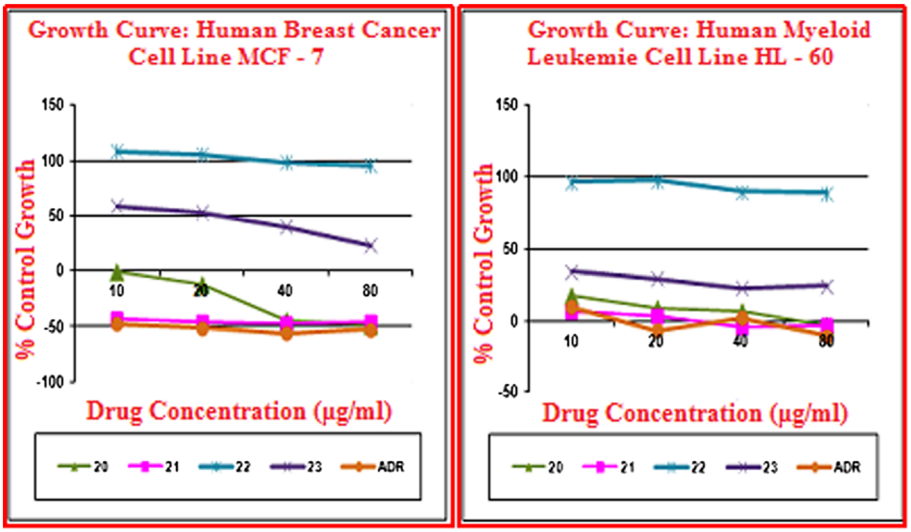

FIGURE 7 Growth curve showing control growth versus drug concentration against MCF-7 and HL-60 cell lines

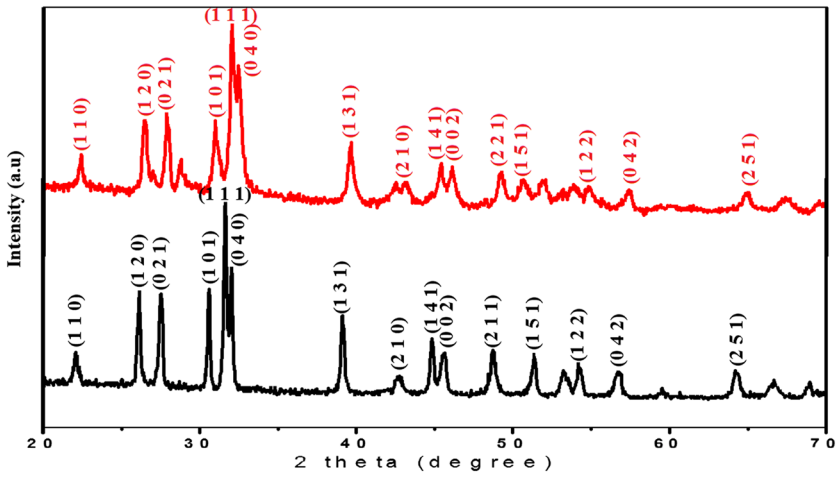

FIGURE 8 Powder XRD patterns of (a) SnS-1 and (b) SnS-2

peaks for both samples are indexed and assigned to SnS of orthorhombic structure with lattice parameters $a = 0.4328$ nm, $b = 0.1119$ nm and $c = 0.3978$ nm (JCPDS 39-0354; herzenbergite). The diffraction peaks at 22.43°, 26.38°, 27.89°, 32.24°, 39.77°, 42.77°, 45.40°, 46.35°, 49.18°, 51.26°, 54.08°, 57.47°, 65.01° and 67.28° correspond to the (1 1 0), (1 2 0), (0 2 1), (1 1 1), (1 3 1), (2 1 0), (1 4 1), (0 0 2), (2 2 1), (1 5 1), (1 2 2), (0 4 2), (2 5 1) and (0 8 1) planes of orthorhombic SnS. In the XRD patterns of both samples, no characteristic peaks was observed for other phases of SnS and impurities such as Sn metal and SnS_2, which indicates that the products are single-phase SnS. HRTEM images of SnS-1 and SnS-2 are displayed in Figure 9. SnS-1 and SnS-2 samples are composed of large numbers of spherical particles with an average size of *ca* 5 and *ca* 2 nm, respectively. The HRTEM image of SnS-1 (Figure 9(b)) exhibits well-defined lattice fringes with a lattice spacing of 0.28 nm, which corresponds to the (1 1 1) plane of orthorhombic SnS. The selected area electron diffraction spots (Figure 9) of both SnS-1 and SnS-2 indicate the crystalline nature of as-prepared SnS nanoparticles.

The formation of SnS was confirmed using EDS analysis. The EDS spectra of SnS-1 and SnS-2 are displayed in Figure S20. The EDS analysis of both the samples confirms the presence of Sn and S in the products. The atomic ratio of Sn and S for SnS-1 (1.0:1.2) and SnS-2 (1.0:1.1) shows that there are some vacancies of Sn^{2+} ion positions or some sulfur dangling bonds are present in SnS-1 and SnS-2.

The Kubelka–Munk method based on diffuse reflectance spectra was employed to determine the band gaps of the samples. Plots of $(F(R)hv)^2$ versus photon energy (hv) are shown in Figure 10. The optical band gaps of the SnS-1 and SnS-2 nanoparticles were estimated from the intercept of the straight part of the curves with the x-axis. The band gap energy values for SnS-1 and SnS-2 are 3.5 and 2.2 eV, which are higher compared to the bulk

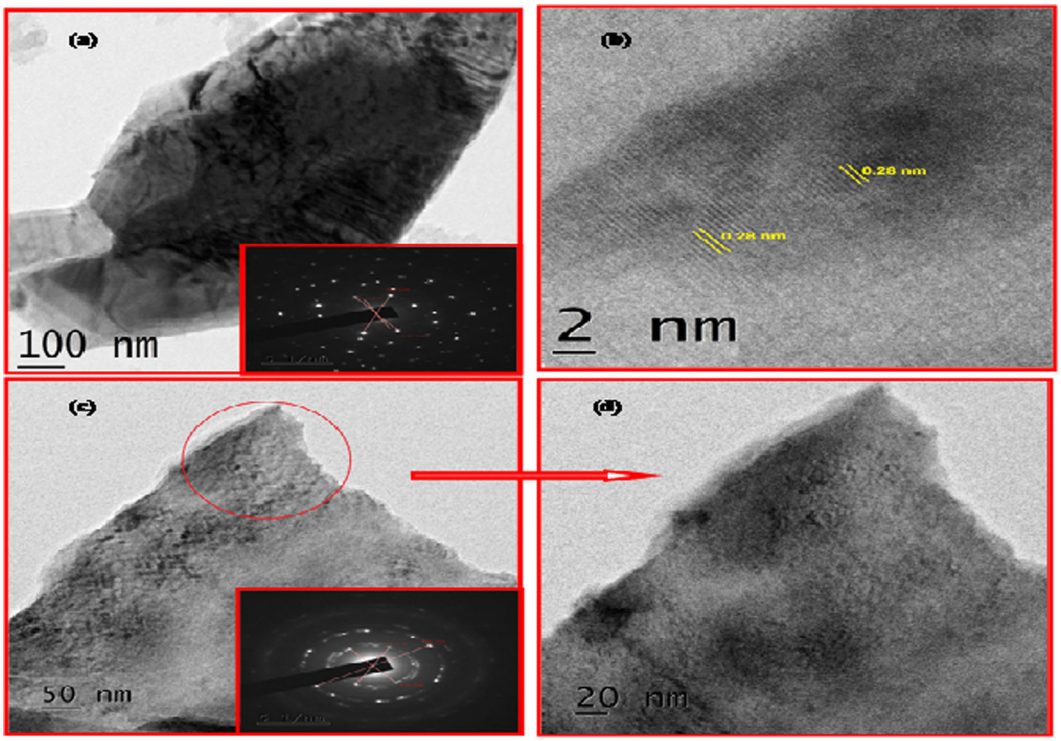

FIGURE 9 HRTEM images and selected area electron diffraction patterns (insets) of SnS-1 and SnS-2

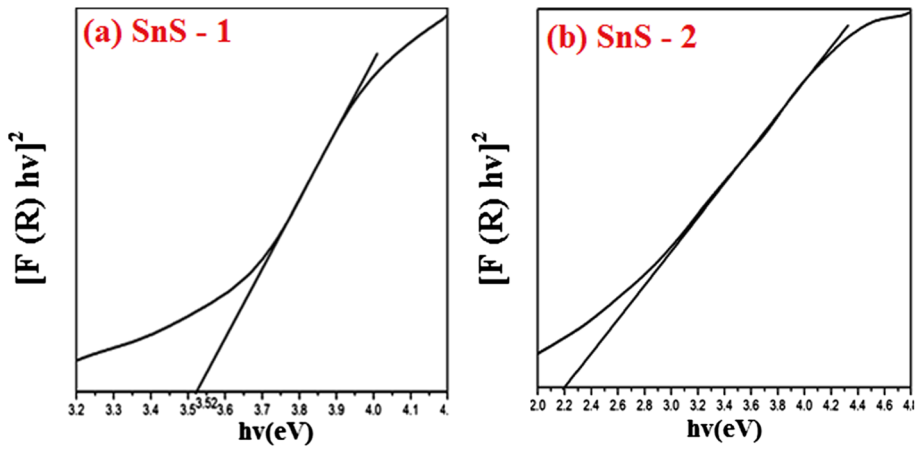

FIGURE 10 UV diffuse reflectance spectra of (a) SnS-1 and (b) SnS-2

SnS band gap (1.3 eV).[49] This indicates quantum confinement effects in the nanoparticles, i.e. when the electron–hole pair is squeezed below the dimensions approaching the exciton Bohr radius.

3.5 | CONCLUSIONS

Four dinuclear macrocyclic complexes, $[Bu_2Sn(dtc)]_2$, have been synthesized. The structures of **1–4** were determined by single-crystal X-ray crystallography. The coordination geometry about the tin atom is skew trapezoidal bipyramid. The anticancer activity of **1–4** decreases in the following order:**1** ≈ **2** > **4** > **3**. Complexes **1** and **3** were used as single-source precursors for the preparation of SnS. Anticancer studies of complexes **1–4** showed that **1** and **2** exhibit better anticancer activity than **3** and **4**. This indicates that the halogen-containing nitrogen-bound organic moiety present in dithiocarbamate ligands increases the anticancer activity of **1** and **2**. This study shows that increasing the number of halogen atoms on organic moiety of dithiocarbamate may increase the anticancer activity of the complexes. The thermal decomposition of complexes **1** and **3** yielded spherical

tin sulfide nanoparticles. The size of tin sulfide nanoparticles in SnS-1 is larger than those in SnS-2. The difference in band gap between SnS-1 and SnS-2 is 1.3 eV. These results indicate that various sizes of tin sulfides with different band gap energy can be prepared using tin dithiocarbamate complexes.

SUPPLEMENTARY DATA

CCDC 1887271–1887274 contain the supplementary crystallographic data for complexes **1**–**4**, respectively. These data can be obtained free of charge via http://www.ccdc.cam.ac.uk/conts/retrieving.html, or from the Cambridge Crystallographic Data Centre, 12 Union Road, Cambridge CB2 1EZ, UK; fax: (+44) 1223–336-033; or e-mail: deposit@ccdc.cam.ac.uk.

ORCID

Subbiah Thirumaran https://orcid.org/0000-0002-5771-5328

REFERENCES

[1] I. Haidnc, *Comprehensive Coordination Chemistry*, Vol. 1, Elsevier, Oxford **2004** 349.

[2] L. A. Komarnisky, R. J. Christopherson, *Nutrition* **2003**, *19*, 54.

[3] P. J. Heard, *Prog. Inorg. Chem.* **2005**, *53*, 1.

[4] G. Hogarth, *Prog. Inorg. Chem.* **2005**, *53*, 71.

[5] G. D. Thorn, R. A. Ludwig, *The Dithiocarbamates and Related Compounds*, Elsevier, New York **1962**.

[6] P. J. Nieuwenhuizen, J. Reedijik, M. Van Duin, W. McGill, *Rubber Chem. Technol. Rubber Rev.* **1997**, *70*, 368.

[7] R. J. Magee, J. D. Hill, *Rev. Anal. Chem.* **1985**, *8*, 5.

[8] N. M. Gandhi, C. K. K. Nair, *J. Radiat. Res.* **2004**, *45*, 175.

[9] S. Tamilvanan, G. Gurumoorthy, S. Thirumaran, S. Ciattini, *Polyhedron* **2017**, *121*, 70.

[10] N. L. Pickett, P. O'Brien, *Chem. Rec.* **2001**, *1*, 467.

[11] E. R. T. Tiekink, *Appl. Organometal. Chem.* **2008**, *22*, 533.

[12] J. O. Adeyemi, D. C. Onwudiwe, M. Singh, *J. Mol. Struct.* **2019**, *1179*, 366.

[13] A. G. Davies, M. Gielen, K. Pannel, E. R. T. Tiekink, *Tin Chemistry: Fundamentals and Frontiers*, Wiley, Chichester.

[14] A. Kumar, A. Singh, R. Yadav, S. Singh, G. Kociok-Köhn, M. Trivedi, *Inorg. Chim. Acta* **2018**, *471*, 234.

[15] S. A. A. Nami, A. Husain, I. Ullah, *Spectrochim. Acta A.* **2014**, *118*, 380.

[16] V. Pillai, S. K. Patel, L. Buch, V. K. Singh, *Appl. Organometal. Chem.* **2018**, *32*, C4559.

[17] J. Cookson, P. D. Beer, *Dalton Trans.* **2007**, 1459.

[18] G. Carpinteyro-López, J. L. Alcántara-Flores, D. Ramírez-Rosales, R. Escudero, B. M. Cabrera-Vivas, S. Bernès, R. Zamorano-Ulloa, Y. Reyes-Ortegaa, *ARKIVOC* **2008**, 19.

[19] T. P. Lockhart, W. F. Manders, E. O. Schlemper, J. J. Zuckerman, *J. Am. Chem. Soc.* **1985**, *108*, 4074.

[20] A. K. Mohamed, N. Auner, M. Bolte, *Acta Crystallogr.* **2003**, *E59*, m190.

[21] N. W. Alcock, J. Culver, S. M. Roe, *J. Chem. Soc. Dalton Trans.* **1992**, 1477.

[22] K. Kim, J. A. Ibers, O. S. Jung, Y. S. Sohn, *Acta Crystallogr.* **2317**, *1987*, C43.

[23] S. W. Ng, C. Wei, V. G. Kumar Das, G. B. Jameson, R. J. Butcher, *J. Organometal. Chem.* **1989**, *365*, 75.

[24] M. Nath, S. Pokharia, R. Yadav, *Coord. Chem. Rev.* **2001**, *215*, 99.

[25] L. Nagy, A. Szorcsik, K. Kovacs, *Acta Pharm. Hung.* **2000**, *70*, 53.

[26] E. Santacruz-Jua'rez, J. Cruz-Huerta, I. F. Herna'ndez-Ahuactzi, R. Reyes-Martinez, H. Tlahuext, H. Morales-Rojas, H. Ho pfl, *Inorg. Chem.* **2008**, *47*, 9804.

[27] J. P. Fuentes-Martinez, I. Toledo-Martinez, P. Roman-Bravo, P. G. Garcia, C. Godoy-Alcantar, M. Lopez-Cardoso, H. Morales-Rojas, *Polyhedron* **2009**, *28*, 3953.

[28] A. N. Gupta, V. Kumar, V. Singh, A. Rajput, L. B. Prasad, M. G. B. Drew, N. Singh, *J. Organometal. Chem.* **2015**, *787*, 65.

[29] J. Cruz-Huerta, M. Carillo-Morales, E. Santacruz-Juarez, I. F. Hernandez-Ahuactzi, J. Escalante-Garcıa, C. Godoy-Alcantar, J. A. Guerrero-Alvarez, H. Hopfl, H. Morales-Rojas, M. Sanchez, *Inorg. Chem.* **2008**, *47*, 9874.

[30] M. G. Vasquez-Rios, V. Reyes-Marquez, H. Hopfl, A. Torres-Huerta, J. Guerrero-lvarez, M. Sanchez, I. F. Hernandez-Ahuactzi, K. Ochoa-Lara, A. Jimenez-Sanchez, R. Santillan, *Eur. J. Inorg. Chem* **2016**, *2016*, 3429.

[31] J. P. Singh, R. K. Bedi, *Thin Solid Films* **1991**, *199*, 9.

[32] M. Parenteau, C. Carlone, *Phys. Rev. B* **1990**, *41*, 5227.

[33] J. B. Johnson, H. Jones, B. S. Lathan, J. D. Parker, R. D. Engelken, C. Barber, *Semicond. Sci. Technol.* **1999**, *14*, 501.

[34] M. Radot, *Rev. Phys. Appl.* **1977**, *18*, 345.

[35] P. Pramanik, P. K. Basu, S. Biswas, *Thin Solid Films* **1987**, *150*, 269.

[36] K. Ramasamy, V. L. Kuznetsov, K. Gopal, M. A. Malik, J. Raftery, P. P. Edwards, P. O'Brien, *Chem. Mater.* **2013**, *25*, 266.

[37] B. P. Bade, S. S. Garje, Y. S. Niwate, M. Afzaal, P. O'Brien, *Chem. Vap. Deposition* **2008**, *14*, 292.

[38] G. Barone, T. Chaplin, T. G. Hibbert, A. T. Kana, M. F. Mahon, K. C. Molloy, I. D. Worsley, I. P. Parkin, L. S. Price, *J. Chem. Soc. Dalton Trans.* **2002**, 1085.

[39] G. M. Sheldrick, *Acta Crystallogr. A* **2008**, *64*, 112.

[40] L. Ronconi, L. Giovagnini, C. Marzano, F. Bettio, R. Graziani, G. Pilloni, D. Fregona, *Inorg. Chem.* **2005**, *44*, 1867.

[41] F. Bonati, R. Ugo, *J. Organometal. Chem.* **1967**, *10*, 257.

[42] H. D. Yin, C. H. Wang, C. L. Ma, *Chin. J. Struct. Chem.* **2004**, *23*, 316.

[43] V. J. Hall, E. R. T. Tiekink, *Main Group Met. Chem.* **1998**, *21*, 245.

[44] J. Holecek, M. Nadvornik, K. Handlir, A. Lycka, *J. Organometal. Chem.* **1986**, *315*, 299.

[45] J. O. Adeyemi, D. C. Onwudiwe, E. C. Hosten, *J. Saudi Chem. Soc.* **2018**, *22*, 427.

[46] M. Mahato, S. MuKherji, K. V. Hecke, K. Harms, A. Ghosh, H. P. Nayek, *J. Organometal. Chem.* **2017**, *853*, 27.

[47] S. K. Sengupta, S. Kumar, *Thermochim. Acta* **1984**, *72*, 349.

[48] A. Bondi, *J. Phys. Chem.* **1964**, *68*, 441.

[49] J. R. S. Brownson, C. Georges, G. Laramona, A. Jacob, B. Delatouche, C. J. Levy-clement, *J. Electrochem. Soc.* **2008**, *155*, D40.

SUPPORTING INFORMATION

Additional supporting information may be found online in the Supporting Information section at the end of the article.

How to cite this article: Selvaganapathi P, Thirumaran S, Ciattini S. Synthesis, spectra, crystal structures and anticancer studies of 26-membered macrocyclic dibutyltin(IV) dithiocarbamate complexes: Single-source precursors for tin sulfide nanoparticles. *Appl Organometal Chem*. 2019;e5089. https://doi.org/10.1002/aoc.5089